ACS OMEGA

Open Access

http://pubs.acs.org/journal/acsodf

Article

Experimental Study on the Dielectric Properties of Coal In Situ with Variable Temperatures

An Zhang, Baoshan Jia,* Huiyao Wang, and Qinai Zhou

Cite This: *ACS Omega* 2024, 9, 19481−19492

Read Online

ACCESS | Metrics & More | Article Recommendations

ABSTRACT: The aim of this study was to explore the mapping relationship between the temperature and the dielectric parameters of coal and rock under variable temperatures as well as to determine the characteristics of a dielectric anomaly response. Experiments were performed using lignite, nonstick coal, gas coal, coking coal, and anthracite. The evolution of pyrolysis characteristics, microcrystal structure, and dielectric properties with changing temperature was investigated, and the changes in the dielectric parameters of coal and rock were comprehensively analyzed. As such, the cause of the dielectric anomaly with changing temperatures of coal and rock was revealed. The results show that the dielectric properties of coal at different pyrolysis temperatures are closely related to the degree of intermolecular thermal motion, the evolution of microcrystal structure, and the mechanism of polarization response. In the low-temperature stage, the thermal motion of coal molecules is weak and exhibits electronic polarization, and the dielectric parameters change slightly with temperature while being dependent on the moisture content. In the high-temperature pyrolysis stage, the intense molecular thermal motion leads to the breaking of chemical bonds and the release of volatiles; moreover, the distance between aromatic layers of coal decreases, the order of aromatic structure increases, the dipole turning polarization is the main polarization type, and the dielectric response is obvious. When the pyrolysis reaction is basically complete, the dielectric constants of the five coal samples reach the maximum. As the temperature increases continuously, the coal structure is destroyed by the weakening of the thermal motion of the coal molecules and the accumulation of thermal stress; meanwhile, the dielectric constant decreases gradually, while the dielectric loss and tangent of dielectric loss increase rapidly. At the same temperature, the dielectric constant decreases with an increase in test frequency. These results lay a foundation for the inversion of dielectric data in fire areas of coal mines.

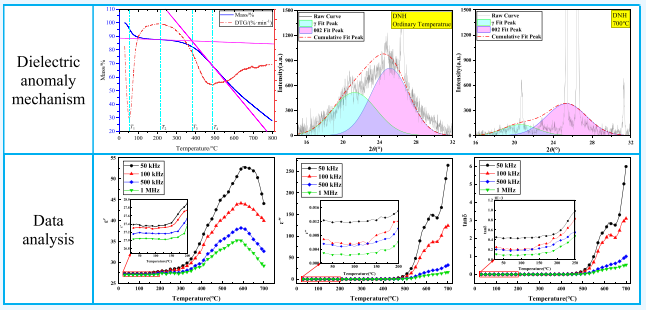

1. INTRODUCTION

Spontaneous coal combustion is a major disaster in coal mines around the world.[1,2] Researchers have noted that spontaneous coal combustion areas are mostly difficult to find;[3,4] moreover, spontaneous coal combustion not only leads to a wastage of substantial coal resources but also causes surface subsidence, land desertification, groundwater and air pollution, and other disasters.[5−9] Coal fire prevention and control works are necessary for the protection of coal resources and the ecological environment and reduction of carbon emissions, which are crucial to achieving the goal of "double carbon".[10]

Before implementing a fire prevention and extinguishing plan, things to know in advance include the characteristics of the temperature distribution in the fire area and the location of hidden fire sources. One of the ways in which a fire source is detected is the use of geological radar exploration technology,[11−13] and the signals collected through this method can reflect the changes in the dielectric parameters of underground coal.[14] The electromagnetic wave emitted by the radar is discontinuous in a nonuniform medium. Owing to the complex underground geological structure, the target detection is obstructed by the surrounding environment and temperature, which easily causes misjudgment and multiple solutions.[15] The reflected wave received by the radar is a function of the medium's dielectric constant. Similarly, the image interpretation, recognition, and inversion all depend on the dielectric properties of the medium.[16] If we can obtain the mapping relationship between the dielectric properties and temperature of coal during combustion heating, then we can perform a finite difference time domain forward modeling of the spatial distribution of a coal fire; thus, we can calculate the spatial location of the fire source using measured data[17] and improve the accuracy of target identification and resolution in GPR imaging. Several scholars have investigated the dielectric

Received: January 30, 2024
Revised: April 6, 2024
Accepted: April 9, 2024
Published: April 18, 2024

Table 1. Proximate Analysis of Five Coal Samples

samples	serial number	proximate analysis (wt %) M_{ad}	A_{ad}	V_{ad}	FC_{ad}	coal rank
Dananhu	DNH	15.23	8.76	27.86	48.15	lignite
Halagou	HLG	9.26	1.79	28.27	60.68	nonstick coal
Hongshiwan	HSW	1.98	8.25	32.28	58.49	gas coal
Xinlu	XL	2.15	8.45	29.35	60.05	coking coal
Xintian	XT	4.18	17.61	4.84	73.37	anthracite

characteristics of coal and rock. For instance, Xu[18] found that the dielectric constant of coal from 25 to 120 °C decreases with increasing temperature, with the value decreasing initially and increasing with the increase in coal grade. Marland et al.[19] found that the dielectric constant and dielectric loss of coal decreased greatly between 80 and 180 °C, which was attributed to the evaporation of water in coal. Because low-rank coal has a high water content, its dielectric factor is higher than that of high-rank coal.[20] Peng et al.[21,22] studied the dielectric characteristics of bituminous coal and anthracite. They found that the dielectric parameters increased as the heat treatment temperature of the coal samples increased. This increase was related to chemical bond breakage and volatile removal during pyrolysis. Xu et al.[23,24] found that the ordered microcrystalline structure of coal increases the dielectric constant and dielectric loss tangent as temperature increases. To date, only a few studies have investigated the measurement and analysis of the dielectric parameters of coal and rock mass under a variable temperature. No studies have explored the characteristics of the dielectric anomalies of coal and rock at variable temperatures, which limits the accuracy of dielectric data inversion in fire areas.

In this study, five metamorphic coals were selected as the research objects, including lignite, nonstick coal, gas coal, coking coal, and anthracite. Experiments were conducted on the microcrystal structure of coal before and after high-temperature treatments. Additionally, the pyrolysis characteristics and dielectric parameters were tested under a variable temperature. The evolution law of the dielectric characteristic parameters of coal under a variable temperature was analyzed, and the internal change mechanism was revealed. These experimental results lay a theoretical foundation for the inversion and analysis of the data on coal mine fire areas, enhancing the accuracy of locating fire areas.

2. EXPERIMENTAL PROCEDURES

2.1. Coal Sample Characterization and Preparation. Five kinds of coal samples were selected from Danan Lake (lignite), Halagou (nonstick coal), Hongshiwan (gas coal), Xinlu (coking coal), and Xintian (anthracite). An MAG-6700 automatic industrial analyzer was used to analyze the raw coal samples, as shown in Table 1. After manual and sieving pretreatment of the raw coal, pulverized coal with a particle size of less than 80 μm was screened and placed in a sealed bag.

Figure 2. High-temperature dielectric temperature spectrum test system.

The prepared coal powder was flaked into a coal type with a diameter of 10 mm and a thickness of 2 mm under a pressure of 11 MPa using a powder flaking machine. To achieve accurate experiments, a layer of conductive silver paste was uniformly coated on the upper and lower surfaces of the sample as a measuring electrode, which was used as the specimen for performing the electrical properties test of the coal, as shown in Figure 1.

Figure 1. Coal coated with conductive silver paste.

2.2. Coal Char Thermogravimetric Analysis. The thermal analysis experiments of the coal were performed using an STA6000 comprehensive thermal analyzer, and five coal samples with a particle size of less than 80 μm were prepared, weighed (10 ± 0.5 mg), and put into a crucible to prepare for the test. The testing conditions of the instrument were an initial temperature of 30 °C, termination temperature of 800 °C, and heating rate of 10 °C/min. Helium gas was passed into the testing chamber as a protective gas with a ventilation volume of 50 mL/min. The temperature accuracy and sensitivity of the thermogravimetric analyzer were 0.1 °C and 0.1 μg, respectively.

2.3. X-ray Diffraction Analysis. Five coal samples with different metamorphic degrees were heat-treated at 700 °C by weighing 10 g. Five raw coal samples and coal samples after heat treatment at 700 °C were tested by using a D8Adange X-ray diffraction instrument (Bruker Company, Germany). The voltage of the X-ray tube of the instrument was 40 kV, the current 30 mA, the detection range (2θ) 5−90°, the scanning speed 10°/min, the anode target material Cu target, the radiation Kα, and the X-ray wavelength 0.15406 nm. The reproducibility of the angle was 0.0001°.

https://doi.org/10.1021/acsomega.4c00954
ACS Omega 2024, 9, 19481−19492

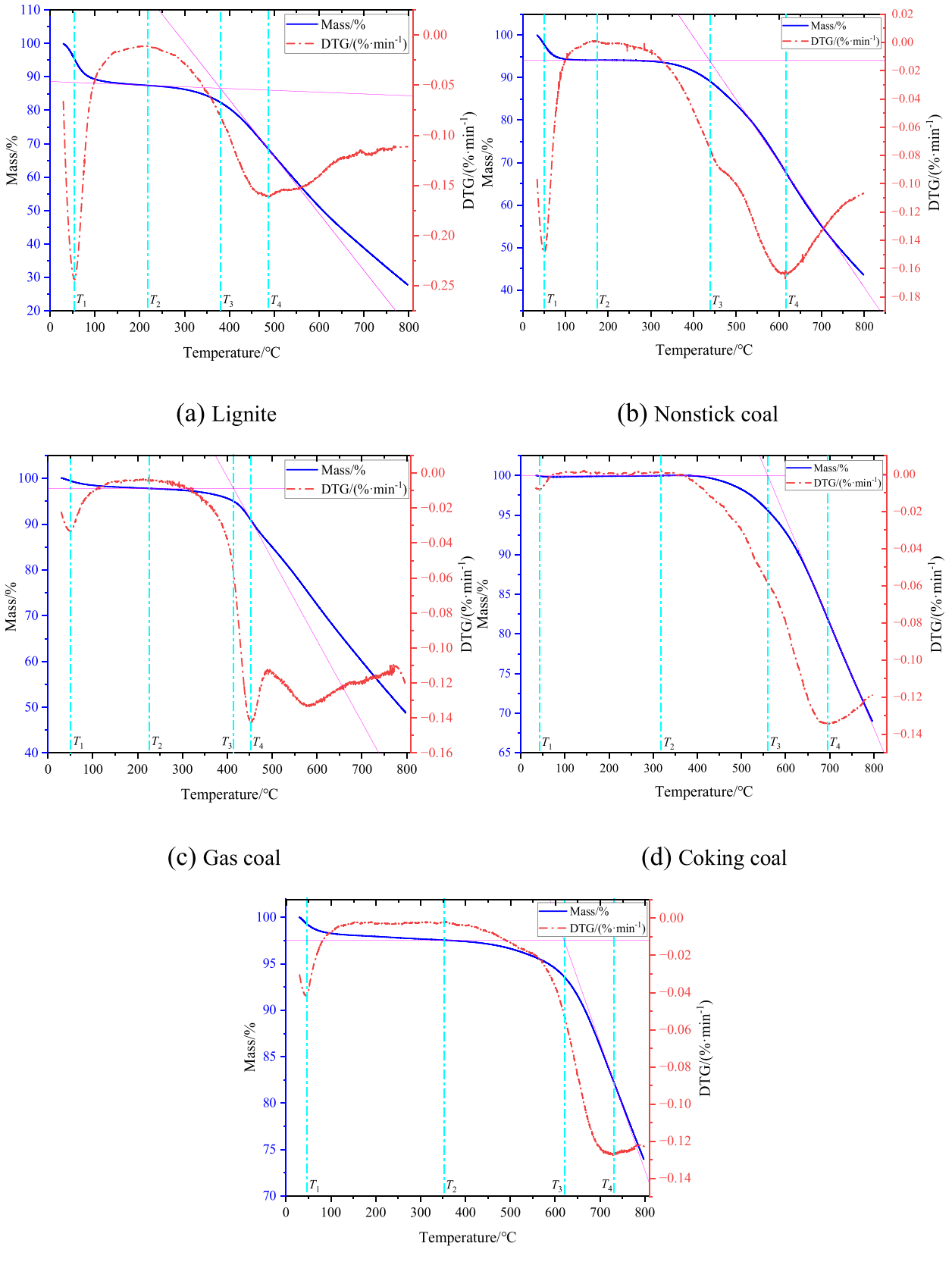

Figure 3. (a–e) TG–DTG curve of pyrolysis of coal with different metamorphic degrees.

https://doi.org/10.1021/acsomega.4c00954
ACS Omega 2024, 9, 19481−19492

The coal microcrystalline structural parameters, facet spacing d_{002}, stacking degree L_c, ductility L_a, average number of aromatic layers N_{ave}, and graphitization g were obtained using the Braggs and Scherrer formulas:[25,26]

$$d_{002} = \frac{\lambda}{2\sin\theta_{002}} \quad (1)$$

$$L_c = \frac{0.89\lambda}{\beta_{002}\cos\theta_{002}} \quad (2)$$

$$L_a = \frac{1.84\lambda}{\beta_{100}\cos\theta_{100}} \quad (3)$$

$$N_{ave} = \frac{L_c}{d_{002}} + 1 \quad (4)$$

$$g = \frac{a_1 - d_{002}}{a_1 - a_2} \quad (5)$$

where λ is the X-ray wavelength of 0.15406 nm, θ_{002} is the diffraction angle of 002 peak, β_{002} is the width of the 002 peak, θ_{100} is the diffraction angle of 100 peak, β_{100} is the width of 100 peak, a_1 is the maximum directional layer spacing of 0.3975 nm in the initial state, and a_2 is the facet spacing of the perfect graphite crystal 0.3354 nm.

2.4. Tests and Calculations of the Dielectric Properties of Coal. In this study, the high-temperature dielectric-spectrum test system, as shown in Figure 2, was used to test the in situ dielectric characteristic parameters of the five coal samples with different metamorphic degrees under different electric field frequencies. The test system consisted of an infrared reflection furnace, a water cooler, a vacuum pump, and a WK6500B precision impedance analyzer (basic accuracy: 0.05%, frequency resolution: ≤1 MHz). The experiment was performed using the four-terminal method. The initial temperature was set to 30 °C, the end temperature was 700 °C, the temperature interval between the test points was 10 °C, the heating rate was 3 °C/min, the vacuum pressure in the test cavity was −0.1 MPa, and the accuracy in the test temperature range was less than ±1 °C. The five coal samples smeared with a conductive silver slurry were tested in the experiment, and the applied electric field frequency was set to 50 kHz, 100 kHz, 500 kHz, and 1 MHz.

2.4.1. Dielectric Constant and Dielectric Loss. The dielectric properties of a substance vary with the temperature and microwave frequency. This property is typically expressed as the complex dielectric constant ε:[27,28]

$$\varepsilon = \varepsilon_0\varepsilon_r = \varepsilon_0(\varepsilon' - j\varepsilon'') \quad (6)$$

where $\varepsilon_0 = 8.854 \times 10^{-12}\mathrm{Fm}^{-1}$ is the vacuum dielectric constant, ε_r is the complex relative permittivity, and j is an imaginary unit.

In practice, as most materials have a small absolute dielectric constant, a complex relative dielectric constant is typically used to quantify the dielectric response for convenience. It can be observed that the complex relative dielectric constant consists of two parts: the relative dielectric constant ε' and the relative dielectric loss factor ε''. ε' is a measure of the ability of a dielectric material to store electrical energy, while ε'' quantifies the loss of electrical energy in the material.

2.4.2. Dielectric Loss Tangent. The dielectric loss tangent (tan δ) is a parameter that evaluates the change in the dielectric constant and dielectric loss factor simultaneously. It is defined as the ratio between the relative dielectric loss factor and the relative dielectric constant:[28]

$$\tan\delta = \frac{\varepsilon''}{\varepsilon'} \quad (7)$$

3. RESULTS AND DISCUSSION

3.1. Analysis of Pyrolysis Characteristics of Coal. Figure 3 shows the TG curves and corresponding DTG curves of the five kinds of coal samples. The TG curve shows the mass change of the sample with the temperature. The DTG curve is based on the TG curve as the instantaneous mass loss rate, indicating the mass loss intensity for a certain period.

Table 2. Characteristic Parameters of Pyrolysis

coal samples	T_1 (°C)	T_2 (°C)	T_3 (°C)	T_4 (°C)
lignite	54.3	217.2	380.6	487.2
nonstick coal	50.5	174.8	438.1	616.1
gas coal	50.9	225.9	413.4	452.3
coking coal	41.3	317.4	559.3	695.1
anthracite	45.3	351.8	619.2	731.9

The pyrolysis characteristic parameters reflecting the thermal stability of coal can be inferred from the TG-DTG curve of coal pyrolysis. Examples include the two obvious weight loss peaks T_1 and T_4 in the DTG curve, the initial pyrolysis temperature T_3, and the first weight loss peak T_1, which causes the physical adsorption loss of moisture and small molecular gases in the coal samples.[29] The second weight loss peak T_4 is the temperature point of the maximum weight loss rate, indicating that the pyrolysis intensity of the coal is at a maximum at this temperature. T_2 is the temperature point of the maximum weight loss rate of the DTG curve, and T_3 is the point of intersection of the tangent line near the level in front of the TG step and the curve inflection point as the reference temperature point for the initiation of the weightlessness process. At this stage, the macromolecular structure of coal is destroyed, and the chains and functional groups of a weak bond energy are broken. Additionally, large amounts of carbon dioxide, water, short-chain aliphatic hydrocarbons, and methane are produced. As the temperature increases, the TG curve decreases continuously. This stage is the polycondensation and polymerization stage, wherein hydrogen is the main product.

Table 2 summarizes the characteristic parameters of pyrolysis.

3.2. Analysis of the Microcrystal Structure of Coal. To obtain the characteristic parameters of the microcrystal morphology of coal, it is necessary to fit and analyze the 002 and 100 peaks of coal samples. The peak fitting was performed by using the built-in peak fitting analysis module of Origin 2023, and the Gaussian model was used for the peak shape. The baseline correction, peak searching, and automatic peak fitting steps were used to perform the split peak fitting of the diffraction peak spectrum. By performing a fitting analysis of the XRD spectra of the five coal samples, the combined peak 002 and γ peak were obtained, as shown in Figures 4−8 (among them, Figure 4 for lignite, Figure 5 for nonstick coal, Figure 6 for gas coal, Figure 7 for coking coal, and Figure 8 for anthracite). As the degree of metamorphism of the coal samples increases, the 002 peak gradually shifts to the right,

https://doi.org/10.1021/acsomega.4c00954
ACS Omega 2024, 9, 19481−19492

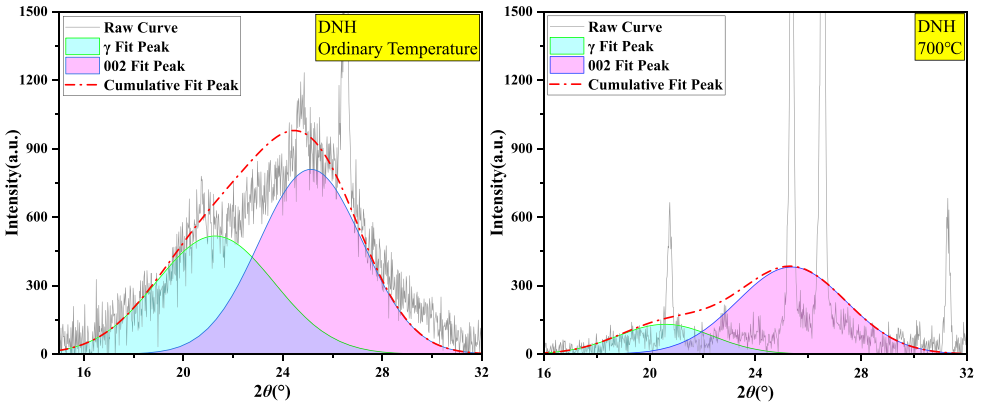

(a) Ambient coal sample (b) 700°C heat-treated coal samples

Figure 4. Fitting diagram of the lignite 002 peak.

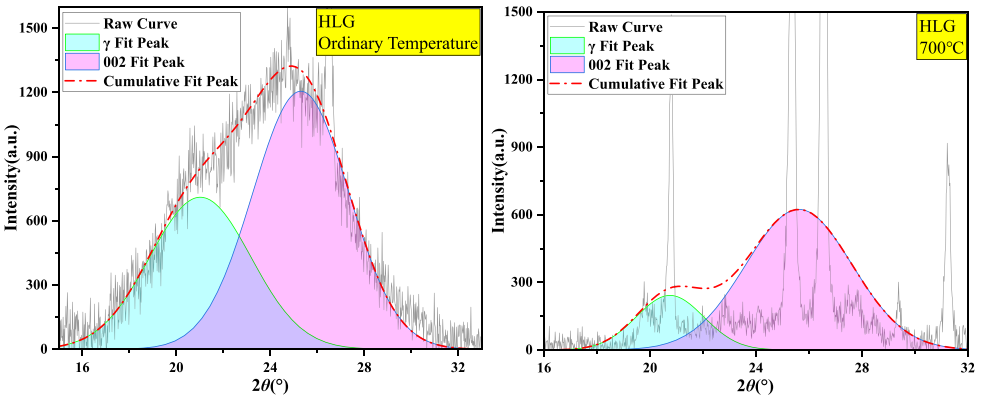

(a) Ambient coal sample (b) 700°C heat-treated coal samples

Figure 5. Fitting diagram of the 002 peak of nonstick coal.

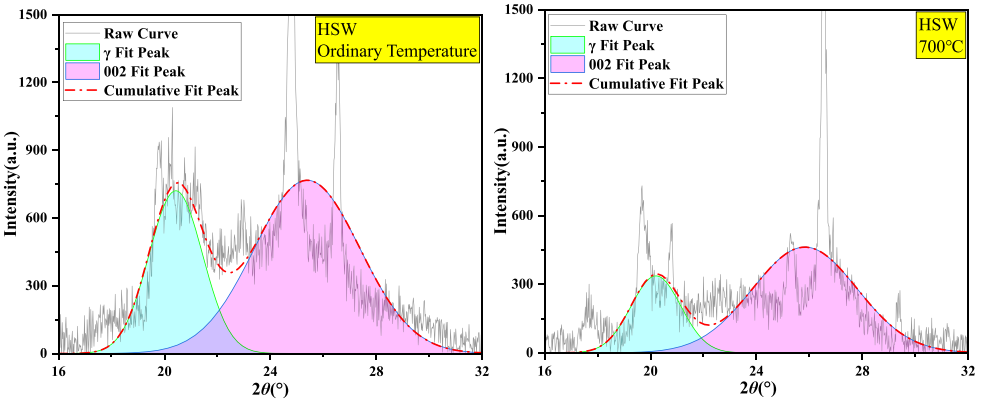

(a) Ambient coal sample (b) 700°C heat-treated coal samples

Figure 6. Fitting diagram of the 002 peak of gas coal.

indicating that metamorphism can change the microcrystalline structure of coal and make it develop toward graphitization.

Formulas 1−5 can be used to obtain the quantitative calculation of the morphological and structural parameters of microcrystals in coal. The results are presented in Table 3; below, we discuss the evolution laws of d_{002}, L_c, L_a, N_{ave}, and g, which are microcrystal structural parameters of raw coal with different metamorphic degrees and coal samples heat-treated at 700 °C.

As shown in Figure 9, the increase in the degree of metamorphism is accompanied by a gradual right shift in the position of the 002 peak of the coal samples heat-treated at room temperature and 700 °C. Accordingly, the distance between aromatic layers in the microcrystal structural unit decreases further, rearranging the carbon layer in the coal microcrystal into a more regular form; moreover, the smaller d_{002} is, the higher the order of the microcrystalline structure is. In general, as coal metamorphism increases, the microcrystal

https://doi.org/10.1021/acsomega.4c00954
ACS Omega 2024, 9, 19481−19492

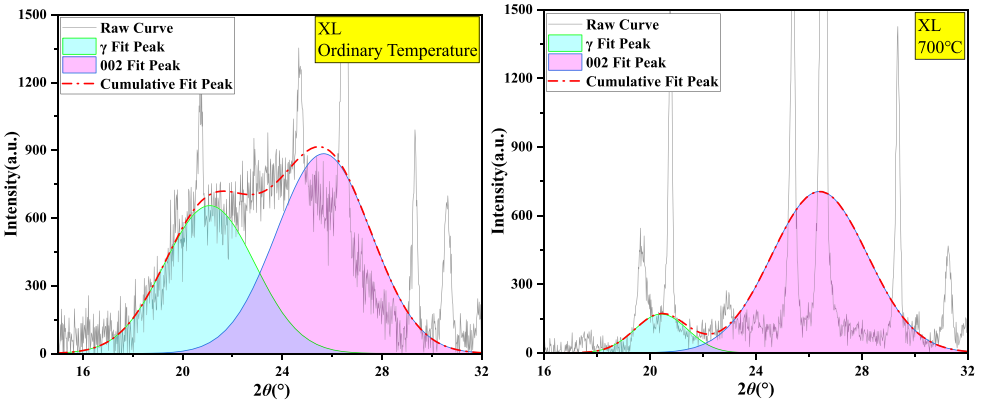

(a) Ambient coal sample (b) 700°C heat-treated coal samples

Figure 7. Fitting diagram of the 002 peak of coking coal.

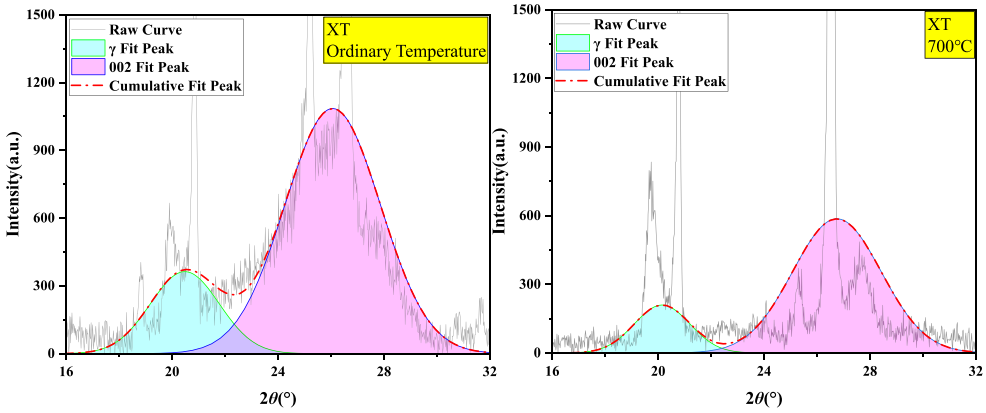

(a) Ambient coal sample (b) 700°C heat-treated coal samples

Figure 8. Fitting diagram of the 002 peak of anthracite.

Table 3. Microcrystalline Structural Parameters of Coal

coal samples	coal sample processing temperature	$2\theta_{002}$ (deg)	$2\theta_{100}$ (deg)	d_{002} (nm)	L_c (nm)	L_a (nm)	N_{ave}	g
lignite	ordinary temperatures	25.13	42.54	0.354084	1.639265	1.475774	5.629588	0.699125
	700 °C	25.37	42.87	0.350789	1.660323	1.486246	5.733112	0.752193
nonstick coal	ordinary temperatures	25.3	42.76	0.351744	1.670427	1.497164	5.748993	0.73682
	700 °C	25.62	43.39	0.347422	1.703286	1.518666	5.902639	0.806405
gas coal	ordinary temperatures	25.39	43.08	0.350517	1.717032	1.528994	5.898571	0.756569
	700 °C	25.83	43.62	0.344645	1.733315	1.552249	6.029275	0.851126
coking coal	ordinary temperatures	25.66	43.42	0.34689	1.802501	1.600885	6.19618	0.814981
	700 °C	26.41	44.16	0.337206	1.894221	1.651941	6.617396	0.970913
anthracite	ordinary temperatures	26.07	44.06	0.341526	1.897366	1.716053	6.555545	0.901345
	700 °C	26.75	44.6	0.332997	2.049502	1.764278	7.154718	1.038696

structure of coal tends toward an improved order, resulting in a higher graphitization degree g of high-rank coal than that of low-rank coal. This phenomenon indicates that obvious polycondensation occurs in the microcrystal structure of the coal's macromolecules under coalification metamorphism, gradually evolving to the direction of graphite crystal. In addition, the stacking degree L_c, ductility L_a, and aromatic layer number N_{ave} of the coal samples exhibit an increasing trend, indicating that coalification promotes the growth of microcrystals and increases the average size of basic structural units. Compared with the coal samples treated at room temperature and 700 °C, a decrease occurs in the distance between aromatic layers of coal samples after the high-temperature treatment decreases. This phenomenon indicates that a closer relationship exists between carbon layers, and the strength of the chemical bonds increases with a temperature rise. The increase in the stacking degree L_c, ductility L_a, and aromatic layer number N_{ave} indicates that more carbon layers are formed In coal. Changes in the coal microcrystal structure affect its dielectric properties, as discussed in the following subsections.

3.3. Analysis of Dielectric Properties and Mechanisms of Coal. The positive and negative charges in the dielectric move under the action of an external electric field, resulting in the deviation of the position of the positive and negative charge centers, the formation of a dipole moment in the dielectrics, and polarization. Specifically, when the external

https://doi.org/10.1021/acsomega.4c00954
ACS Omega 2024, 9, 19481−19492

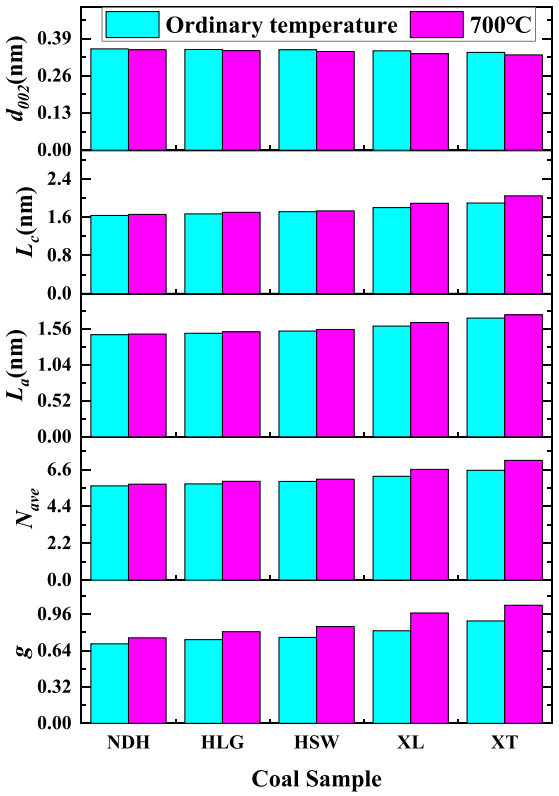

Figure 9. Microcrystalline structural parameters of coal samples heat-treated at room temperature and 700 °C.

electric field and temperature of the dielectric change, the bound charge bound to the atom, molecule, lattice, defect position, or local region produces or alters the electric dipole moment and then produces polarization or a surface-induced charge. The dielectric constant indicates the degree of polarization of the dielectric, that is, the binding ability to the charge. The higher the value, the stronger the binding ability of the dielectric to the charge. Under the action of the electric field, the dielectric loss refers to the energy consumed by dielectrics in unit time due to the hysteresis effect of dielectric conductivity and polarization.

3.3.1. Analysis of Dielectric Characteristics of Coal at Room Temperature. Figure 10 shows the following characteristics for the dielectric parameters of the coal samples with different metamorphic degrees under four test frequencies:

(1) Under different test frequencies, the dielectric constant, dielectric loss factor, and dielectric loss tangent of the coal samples decrease gradually as the test frequency increases. This phenomenon is due to the mismatch between orientation polarization and ion polarization as well as the time of change of the electric field under the action of a high-frequency electric field; thus, it is difficult to establish the polarization process.

(2) As the degree of metamorphism increases, the dielectric constant of coal is lower in the middle and higher on both sides, while the dielectric loss factor and tangent of the dielectric loss increase gradually. The increase in the XT anthracite with the highest metamorphic degree is particularly significant because anthracite has a large and orderly aromatic structure.

(3) According to the data in Table 1, it can be concluded that a certain correlation exists between Mad and the dielectric constant of coal; although the moisture content of anthracite comes third, its dielectric constant is the highest, indicating that the water content is not the decisive factor of dielectric parameters. The FC_{ad} of the fixed carbon content of coal is basically consistent with the numerical fluctuation of its dielectric constant, indicating that FC_{ad} is also a factor affecting the dielectric properties.

3.3.2. Analysis of Dielectric Characteristics of Coal Under the Condition of Variable Temperature In Situ. The polarization type of coal and rock varies with the frequency and temperature of the tested electric field, which affect the dielectric values of coal and rock. The change curves of dielectric constant and dielectric loss factor of five coal samples at different testing frequencies under variable temperature in situ are shown in Figures 11−15(among them, Figure 11 for lignite, Figure 12 for nonstick coal, Figure 13 for gas coal, Figure 14 for coking coal, and Figure 15 for anthracite). Through the analysis of the changing trend of the dielectric parameters, combined with the pyrolysis characteristic temperature presented in Table 2, we obtain the characteristic parameters of the coal dielectric properties under variable temperature conditions (Table 4), which are divided into three stages.

The first stage (stage I) is from 30 °C to $T_{EV\ I}$. The values of $\varepsilon'$and $\varepsilon''$of the coal change only slightly, the polarization is mostly electron polarization and atomic(ion) polarization, the thermal motion between coal molecules is weak, and the dielectric polarization related to thermal motion is not

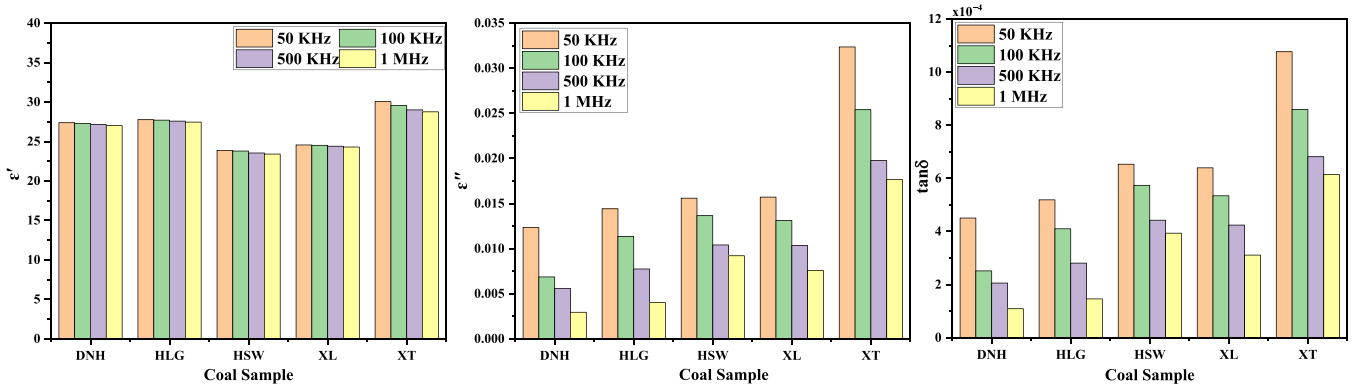

Figure 10. Dielectric characteristics of coal samples of different testing frequencies at room temperature.

https://doi.org/10.1021/acsomega.4c00954
ACS Omega 2024, 9, 19481−19492

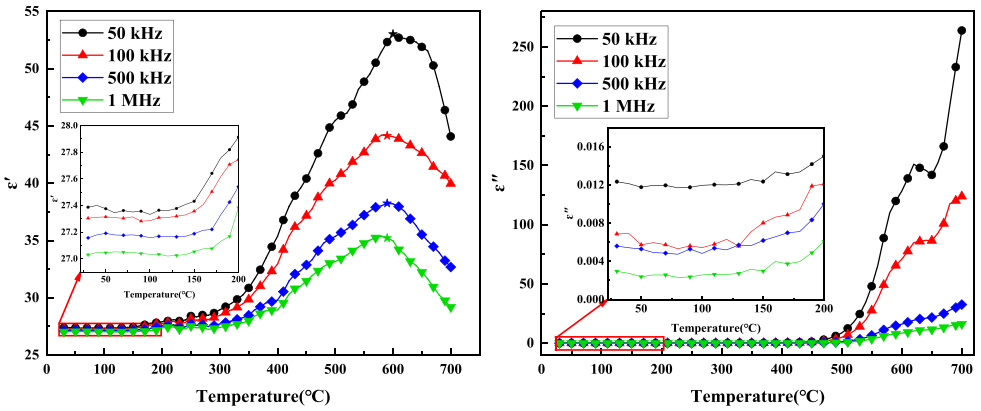

(a) Dielectric constant (b) Dielectric loss

Figure 11. Variation of dielectric properties of lignite with temperature.

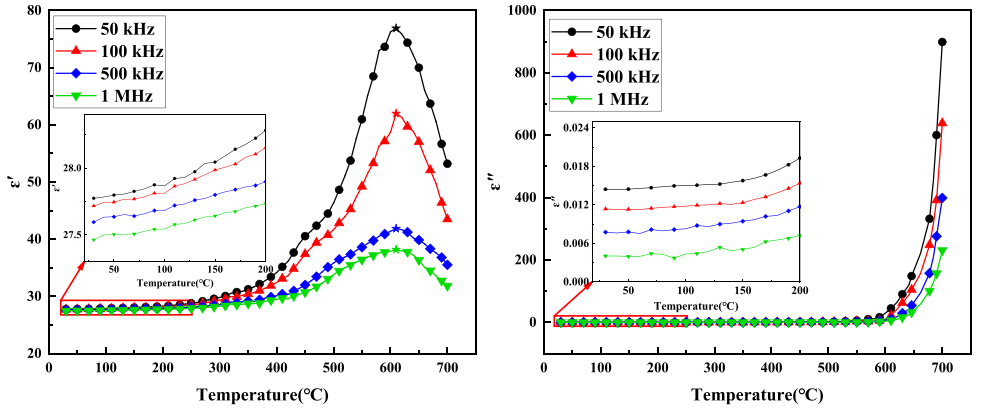

(a) Dielectric constant (b) Dielectric loss

Figure 12. Variation of dielectric properties of nonstick coal with temperature.

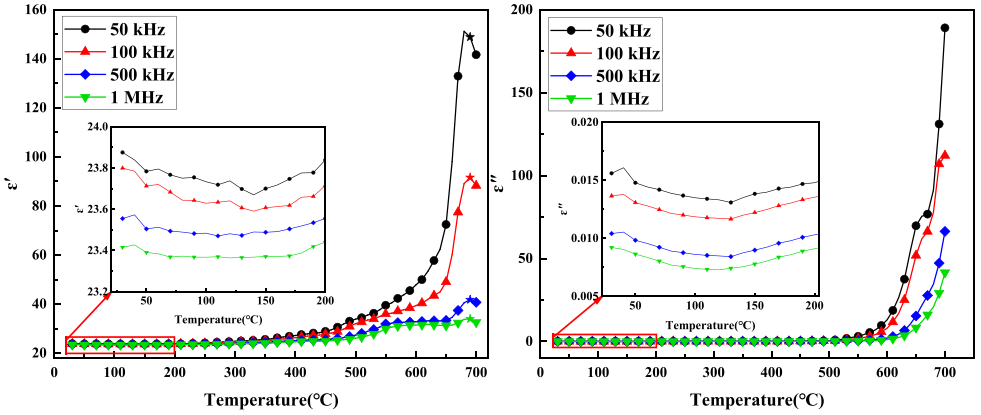

(a) Dielectric constant (b) Dielectric loss

Figure 13. Variation of dielectric properties of gas coal with temperature.

established at this stage. In the initial stage of heating, most of the dielectric parameters of the coal samples decrease slightly, which is due to the evaporation of water adsorbed on the coal and the decrease in electrical conductivity.

The second stage (stage II) is from $T_{EV\ I}$ to $T_{EV\ III}$. The $\varepsilon'$and ε'' values of coal increase gradually. At a temperature of $T_{EV\ II}$, the thermal motion of the coal molecules intensifies at a high temperature, the macromolecular structure disintegrates rapidly, the chemical bond breaks, and volatiles are released gradually. As the temperature increases, the entire molecule and its groups rotate freely. This means that the dipole turning polarization can be established in a very short time, while the polarization time decreases exponentially. The dielectric constant of the four test frequencies of the coal samples peaks when the temperature rises to $T_{EV\ III}$, indicating the occurrence of a major phase transition in this temperature range. At the peak value of ε', the pyrolysis reaction of the coal nears its end, and the thermal motion of the coal molecules

https://doi.org/10.1021/acsomega.4c00954
ACS Omega 2024, 9, 19481−19492

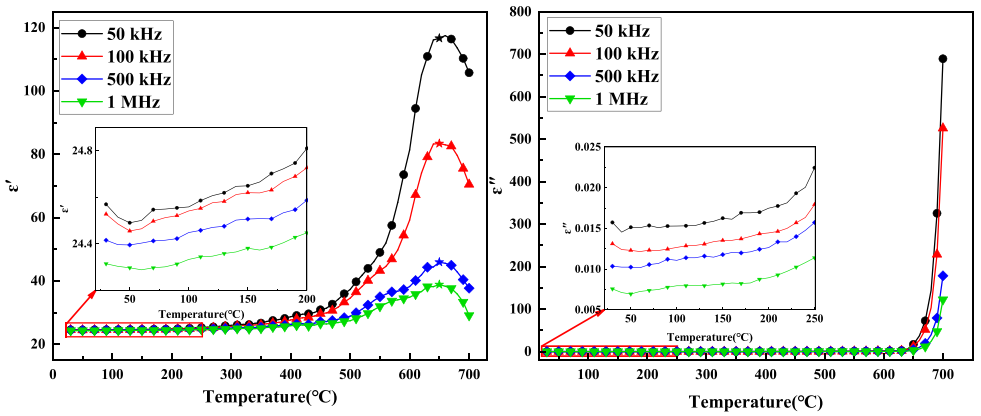

(a) Dielectric constant (b) Dielectric loss

Figure 14. Variation of dielectric properties of coking coal with temperature.

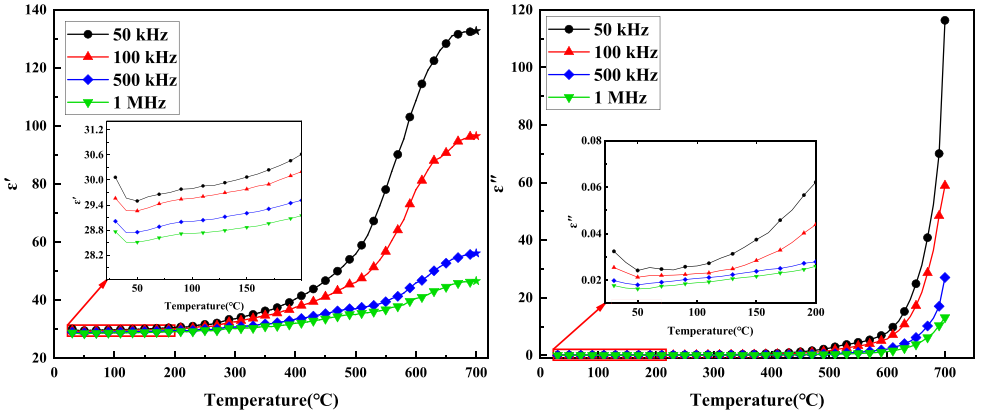

(a) Dielectric constant (b) Dielectric loss

Figure 15. Variation of dielectric properties of anthracite with temperature.

Table 4. Dielectric Characteristic Parameters of Coal under the Condition of Variable Temperature

		eigenvalue I (EV I)			eigenvalue II (EV II)			eigenvalue III (EV III)		
coal samples	FREQ (Hz)	TEMP (°C)	ε'	ε''	TEMP (°C)	ε'	ε''	TEMP (°C)	ε'	ε''
lignite	50 K	210	27.97	0.017	350	30.86	0.121	590	52.32	120.01
	100 K		27.85	0.014		29.86	0.087		44.15	65.60
	500 K		27.58	0.011		28.47	0.047		38.24	14.772
	1 M		27.42	0.007		27.98	0.041		35.21	7.788
nonstick Coal	50 K	180	28.18	0.017	370	32.15	0.124	610	76.88	44.74
	100 K		28.08	0.014		31.01	0.093		61.99	22.27
	500 K		27.86	0.01		29.41	0.054		41.85	11.2
	1 M		27.7	0.007		28.80	0.043		38.18	6.2
gas coal	50 K	230	23.95	0.017	420	27.85	0.077	690	148.87	131.06
	100 K		23.84	0.013		26.9	0.074		91.59	106.93
	500 K		23.64	0.011		25.28	0.048		41.78	47.259
	1 M		23.51	0.010		24.84	0.042		33.94	29.133
coking coal	50 K	310	26.086	0.04	470	32.64	0.246	650	116.62	16.938
	100 K		25.783	0.032		30.641	0.185		83.37	12.101
	500 K		25.174	0.025		27.484	0.1		45.91	4.685
	1 M		24.929	0.018		26.605	0.077		38.85	2.869
anthracite	50 K	270	32.13	0.153	490	54.05	2.147	700	132.72	116.38
	100 K		31.27	0.101		45.46	1.375		96.53	58.967
	500 K		30.02	0.046		37.04	0.432		56.14	27.035
	1 M		29.58	0.039		35.07	0.281		46.57	13.14

https://doi.org/10.1021/acsomega.4c00954
ACS Omega 2024, 9, 19481−19492

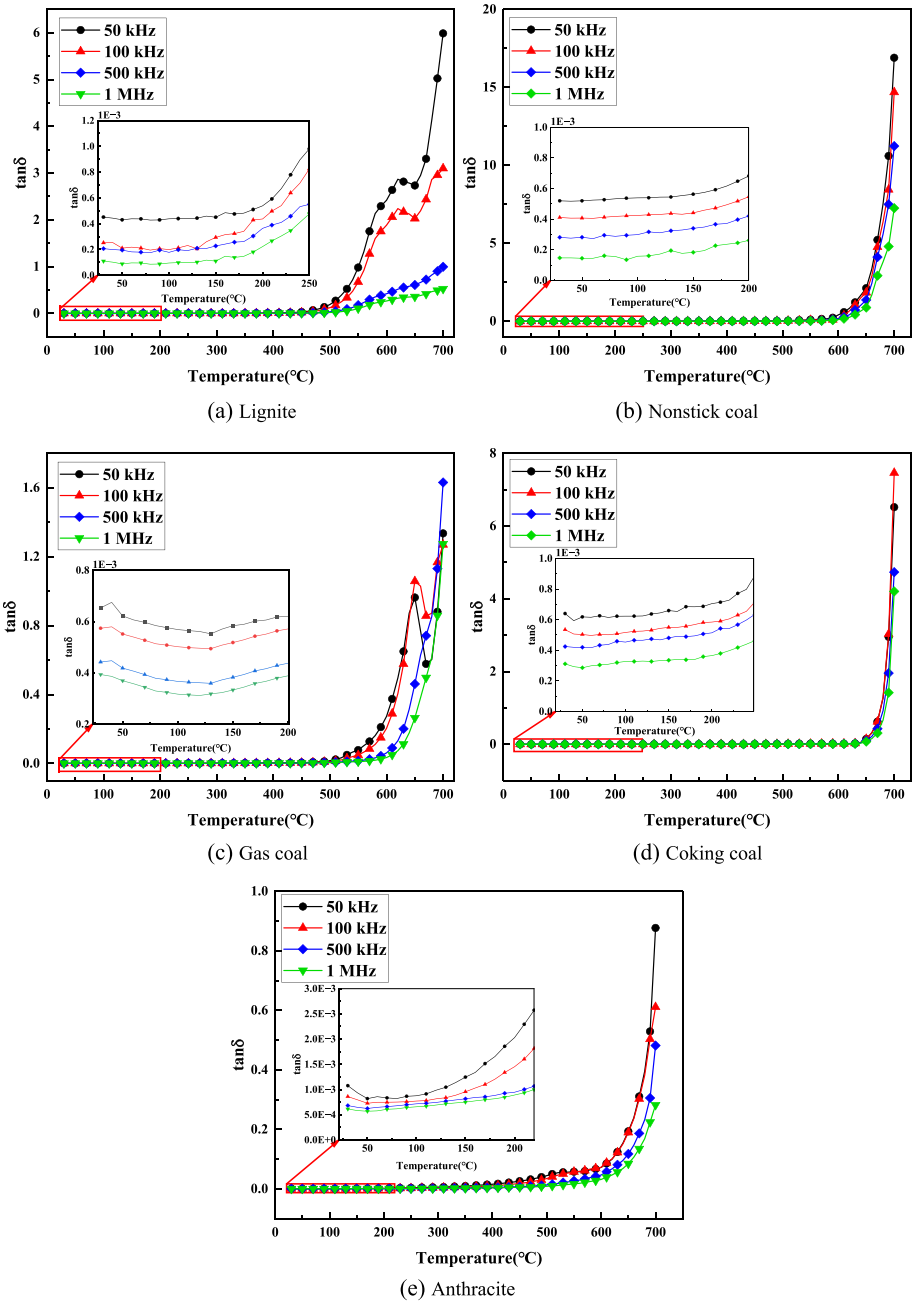

Figure 16. (a−e) Variation of tangent of dielectric loss of coal with temperature.

weakens, accompanied by a gradual increase in the growth rate of the dielectric loss.

The third stage (stage III) is from $T_{EV\ III}$ to 700 °C. At the beginning of this stage, the pyrolysis reaction of coal is basically completed. During the pyrolysis process, chemical bond breakage, and the removal of volatile matter, as well as the accumulation of thermal stress, lead to the destruction of the internal structure of the coal, reducing its ability to hold charges. At high temperatures, dielectric polarization may also cause some dielectric loss. Therefore, the ε' of coal decreases gradually with the increase in temperature, while ε'' increases rapidly. Owing to the high degree of metamorphism and graphitization of anthracite, the pyrolysis reaction is not yet complete when the temperature peaks at 700 °C, and the reduction process of ε' cannot be determined.

Figure 16 shows the temperature dependence of the dielectric loss tangent under the condition of variable temperature in situ and considering the changes in the dielectric constant and loss factor. The change trend is similar to that of the dielectric loss factor, indicating that the dielectric loss factor plays a leading role in the dielectric response of coal. The tangent of dielectric loss increases with an increase in temperature.

3.3.3. Correlation Mechanism of Dielectric Properties of Coal with the Pyrolysis Process and Microcrystalline Structure. The characteristic temperature of coal pyrolysis is an important parameter that describes the pyrolysis characteristics of coal. Coal exhibits different dielectric characteristics at different pyrolysis stages. At the initial stage of pyrolysis, the fluctuation of the dielectric parameters of the coal sample is small and water evaporation is the main influencing factor. In

https://doi.org/10.1021/acsomega.4c00954
ACS Omega 2024, 9, 19481−19492

the T_2-T_3 stage, as the pyrolysis temperature increases, the pyrolysis reaction is enhanced, the thermal motion between molecules and the charge conduction capacity are intensified, and the dielectric parameters increase gradually. When the pyrolysis temperature reaches T_4, the pyrolysis reaction is basically completed and the dielectric constant reaches the maximum.

In terms of the microcrystal structure, the coal sample at room temperature mainly exists in the solid phase, and the coal sample pyrolyzed at 700 °C is in a melting state, reducing the aromatic layer spacing d_{002} while increasing the stacking degree L_c, ductility L_a, and number of aromatic layers N_{ave}. The high temperature leads to a closer relationship between the carbon layers, and the smaller spacing between the aromatic layers enhances the interaction between the aromatic layers, thus increasing the dielectric constant of coal. At the same time, the barrier of charge transfer is increased, and the dielectric loss and tangent of the dielectric loss are increased. A high stacking degree means more contact points between molecules, which helps in increasing the polarization and energy loss; as the extension increases, the interaction between the coal molecules increases, promoting the occurrence of the polarization phenomenon. The increase in graphitization g typically indicates a better aromatic lamellar accumulation and π electron conjugation in coal, increasing the dielectric constant, dielectric loss, and dielectric loss tangent. According to the analysis of the microcrystal structure of coal, an obvious correlation exists between the microcrystal structure parameters and dielectric parameters before and after heat treatment.

4. CONCLUSIONS

In this study, the in situ dielectric properties of lignite, nonstick coal, gas coal, coking coal, and anthracite were measured and analyzed under electric field frequencies of 50, 100, 500, and 1 MHz. The conclusions are summarized as follows:

(1) In the low-temperature stage (30 °C, $T_{EV\ I}$), the thermal motion of coal molecules is weakly electron-polarized, and the dielectric parameters change slightly with changing temperature, decreasing with the evaporation of water in coal for a period of time.

(2) In the high-temperature pyrolysis stage (from $T_{EV\ I}$ to $T_{EV\ III}$), the intense molecular thermal motion leads to the breaking of chemical bonds and the release of volatiles, the distance between the aromatic layers of coal decreases, the order of the aromatic structure increases, the dipole turning polarization can be established rapidly in a short time, and the dielectric response is obvious. As the pyrolysis reaction approaches completion, the dielectric constants of the five coal samples reach the maximum.

(3) When the pyrolysis reaction is completed, the coal structure is destroyed and the charge capacity is reduced because of the weakening of the thermal motion of the coal molecules and the accumulation of thermal stress. The dielectric constant decreases gradually, and the dielectric loss and tangent of the dielectric loss increase rapidly.

(4) At room temperature, as the degree of coal metamorphism increases, the dielectric constant is lower in the middle but higher on both sides, while the dielectric loss and tangent of the dielectric loss increase step by step. Under different electric field frequencies, the dielectric parameters of coal decrease with an increase in frequency.

AUTHOR INFORMATION

Corresponding Author

Baoshan Jia − *College of Safety Science and Engineering and Key Laboratory of Mine Thermo-motive Disaster and Prevention Ministry of Education, Liaoning Technical University, Huludao, Liaoning 125105, China;* orcid.org/0009-0001-2267-5952; Email: jbs1972@126.com

Authors

An Zhang − *College of Safety Science and Engineering and Key Laboratory of Mine Thermo-motive Disaster and Prevention Ministry of Education, Liaoning Technical University, Huludao, Liaoning 125105, China;* orcid.org/0000-0003-4275-5682

Huiyao Wang − *College of Safety Science and Engineering and Key Laboratory of Mine Thermo-motive Disaster and Prevention Ministry of Education, Liaoning Technical University, Huludao, Liaoning 125105, China*

Qinai Zhou − *College of Safety Science and Engineering and Key Laboratory of Mine Thermo-motive Disaster and Prevention Ministry of Education, Liaoning Technical University, Huludao, Liaoning 125105, China*

Complete contact information is available at: https://pubs.acs.org/10.1021/acsomega.4c00954

Notes

The authors declare no competing financial interest.

ACKNOWLEDGMENTS

We are grateful for the financial support of the research from the National Key R&D Project: Coal mine thermal power disaster prevention and control and equipment (no. 2018YFC0807900); we also sincerely thank the editors and anonymous reviewers for improving the quality of this manuscript, as well as MJEditor (www.mjeditor.com) for providing English editing services.

REFERENCES

(1) Deng, J.; Li, B.; Wang, K.; et al. Research status and prospect of coal fire disaster prevention technology in my country. *Coal Sci. Technol.* **2016**, *44* (10), 1−7.

(2) Li, Q. W.; Xiao, Y.; Zhong, K. Q.; et al. Overview of commonly used materials for coal spontaneous combustion prevention[J]. *Fuel* **2020**, *275* (2020), No. 117981.

(3) Kuenzer, C.; Stracher, G. B. Geomorphology of coal seam fires[J]. *Geomorphology* **2012**, *138* (1), 209−222.

(4) Song, Z. Y.; Kuenzer, C. Coal fires in China over the last decade: A comprehensive review[J]. *International Journal of Coal Geology* **2014**, *133* (2), 72−99.

(5) Siddharth, S.; Bhanu, P.; Lal, B. R.; et al. Tree responses to foliar dust deposition and gradient of air pollution around opencast coal mines of Jharia coalfield, India: gas exchange, antioxidative potential and tolerance level. *Environ. Sci. Pollut. Res.* **2021**, *28* (7), 8637−8651.

(6) Cao, F.; Meng, M.; Shan, B.; et al. Source apportionment of mercury in surface soils near the Wuda coal fire area in Inner Mongolia, China[J]. *Chemosphere* **2021**, *263* (2021), No. 128348.

(7) O'Keefe, J. M. K.; Henke, K. R.; Hower, J. C.; et al. CO_2, CO, and Hg emissions from the Truman Shepherd and Ruth Mullins coal fires, eastern Kentucky, USA[J]. *Sci. Total Environ.* **2010**, *408* (7), 1628−1633.

https://doi.org/10.1021/acsomega.4c00954
ACS Omega 2024, 9, 19481−19492

(8) Zhang, Y.; Zhang, X. Q.; et al. Mineralogical and geochemical characteristics of pyrometamorphic rocks induced by coal fires in Junggar Basin, Xinjiang, China[J]. *Journal of Geochemical Exploration* **2020**, *213* (2020), No. 106511.
(9) Wang, H. Y.; Zhang, J. P.; Zhang, L.; et al. Gas Emission and Soil Chemical Properties Associated with Underground Coal Fires, Wuda Coalfield, Inner Mongolia, China[J]. *Natural Resources Research* **2020**, *29* (6), 3973−3985.
(10) Chen, F.; Yu, H. C.; Bian, Z. F.; et al. How to handle the crisis of coal industry in China under the vision ofcarbon neutrality. *J. China Coal Soc.* **2021**, *46* (06), 1808−1820.
(11) Wang, L. C.; Gao, K. Detection of hidden fire source in goaf by ground penetrating radar. *Coal Sci. Technol.* **1998**, *26* (02), 8−10.
(12) Yim, X. B.; Zhang, B.; Deng, J. P.; et al. Application of dielectric parameter numerical experiment to GPR test and detection. *J. Chongqing Univ.* **2016**, *39* (04), 32−40.
(13) Yao, X. C.; Guo, B. X.; Gao, L. V.; et al. Study on Recursive inversion of Permittivity of GPR data. *J. Xi'an Univer. Technol.* **2016**, *32* (02), 199−206.
(14) Yang, F.; Peng, S. P.; Ma, J. W.; et al. Spectral analysis for ground penetrating radar surveys of theunderground coal fire in Wuda Coal Mine. *J.China Coal Soc.* **2010**, *35* (05), 770−775.
(15) Mohamed, E.; Camilla, C.; Elena, G.; et al. In-situ GPR test for three-dimensional mapping of the dielectric constant in a rock mass. *J. Appl. Geophys.* **2017**, *146* (2017), 1−15.
(16) Yao, X. C.; Guo, B. X.; Lv, G.; et al. Recursive inversion research on dielectric permittivity with data by ground penetrating radar. *J. Xi'an Univ. Archit. Technol.* **2016**, *32* (02), 199−206.
(17) Su, L. H.; Li, N.; Lv, G.; et al. Dielectric constant of gravel-soil mixture and FDTD forward analysis of weak zone in tunnels. *Chin. J. Rock Mech. Eng.g* **2015**, *34* (06), 1172−1178.
(18) Xu, H. W. Measurement and test of seam Electrical parameter and study on relationship between seam electric parameter and coal petrology characteristics. *Coal Sci. Technol.* **2005**, No. 03, 42−46.
(19) Marland, S.; Merchant, A.; Rowson, N. Dielectric properties of coal[J]. *Fuel* **2001**, *80* (13), 1839−1849.
(20) Liu, H. Y.; Li, J. X.; Liu, Y. C.; et al. Effect of ash on dielectric properties and micro-structure of high alkali coal at different temperature pyrolysis[J]. *Journal of the Energy Institute* **2020**, *93* (4), 1747−1754.
(21) Peng, Z. W.; Lin, X. L.; Wu, X. J.; et al. Microwave absorption characteristics of anthracite during pyrolysis[J]. *Fuel Process. Technol.* **2016**, *150* (2016), 58−63.
(22) Peng, Z. W.; Hwang, J. Y.; Kim, B. G.; et al. Microwave Absorption Capability of High Volatile Bituminous Coal during Pyrolysis[J]. *Energy fuels* **2012**, *26* (8), 5146−5151.
(23) Xu, L.; Liu, H. Y.; Jin, Y.; et al. Experimental study on dielectric properties of coal under different char-making conditions. *Thermal Power Gener.* **2015**, *44* (04), 11−16.
(24) Xu, L.; Liu, H. Y.; Jin, Y.; et al. Structural order and dielectric properties of coal chars[J]. *Fuel* **2014**, *137* (2014), 164−171.
(25) Pan, R. K.; Li, C.; Yu, M. G.; et al. Evolution patterns of coal micro-structure in environments with different temperatures and oxygen conditions[J]. *Fuel* **2020**, *261* (2020), No. 116425.
(26) Li, H.; Liu, W. C.; Lu, J. X.; et al. Effect of microwave-assisted acidification on the microstructure of coal: XRD, 1H-NMR, and SEM studies[J]. *International Journal of Mining Science and Technology* **2023**, *33* (7), 919−926.
(27) Fan, W.; Jia, C. Y.; Hu, W.; et al. Dielectric properties of coals in the low-terahertz frequency region[J]. *Fuel* **2015**, *162* (2015), 294−304.
(28) Xu, G.; Huang, J. X.; Hu, G. Z.; et al. Experimental study on effective microwave heating/fracturing of coal with various dielectric property and water saturation[J]. *Fuel Process. Technol.* **2020**, *202* (2020), No. 106378.
(29) Jia, L.; Cheng, P.; Yu, Y.; et al. Regeneration mechanism of a novel high-performance biochar mercury adsorbent directionally modified by multimetal multilayer loading[J]. *Journal of Environmental Management* **2023**, *326* (2023), No. 116790.

https://doi.org/10.1021/acsomega.4c00954
ACS Omega 2024, 9, 19481−19492